Elastic anomalies at the first order transition in Lu5Ir4Si10

M. Saint-Paul, Christine Opagiste, C. Guttin

Version of Record: https://www.sciencedirect.com/science/article/pii/S0022369719313800
Manuscript_24f0b392373fa35236c6eefa63817373

Elastic anomalies at the first order transition in $Lu_5Ir_4Si_{10}$

M. Saint-Paul*, C. Opagiste, C. Guttin

Univ. Grenoble Alpes, CNRS, Grenoble INP[a], Institut Néel, 38042 Grenoble, France

Abstract

Ultrasonic measurements on a single crystal of the intermetallic compound $Lu_5Ir_4Si_{10}$ are presented. Large anomalies in the velocity and ultrasonic attenuation of the elastic modes are observed at the structural phase transition T_S~80 K. The velocity of the longitudinal C_{11} and C_{33} mode exhibits a second order transition behavior. In contrast the velocities of the shear C_{44} and C_{66} modes exhibit a first order transition behavior. The longitudinal C_{11} mode is strongly coupled to the ordering system below T_S. Similarities in the longitudinal elastic anomalies with known reduced dimensional charge density wave systems suggest that the nature of the structural phase transition T_S in $Lu_5Ir_4Si_{10}$ could be associated with a charge density wave phase transition.

*michel.saint-paul@neel.cnrs.fr

[a]*Institute of Engineering Univ. Grenoble Alpes*

Keywords: Charge density waves; Intermetallic compounds; Sound velocity; Ultrasonic attenuation.

1. Introduction

The intermetallic compound $Lu_5Ir_4Si_{10}$ exhibits a first-order structural phase transition at T_S ~ 80 K associated with a commensurate lattice modulation along the c axis with a seven-unit cell period [1-8]. This first order phase transition observed in $Lu_5Ir_4Si_{10}$ is characterized by a large specific heat jump, changes in the thermal expansion coefficients, anomalies in the elastic constants and a sudden drop of the electric resistivity [1-7]. Charge modulation should be associated to the structural phase transition T_S but the microscopic origin of this phase transition in this material is still debated and remains controversial [8-15]. This phase transition T_S in $Lu_5Ir_4Si_{10}$ has been denoted by T_{CDW} in references [1-8]. Mansart et al [8] show by ultrafast optical reflectivity measurements a direct involvement of the lattice in the CDW formation and the Peierls origin of multiple charge density waves in $Lu_5Ir_4Si_{10}$. The apparent low value of the order parameter critical exponent $2\beta \sim 0.3$ derived from the temperature dependence of the intensities of satellite reflections in $Lu_5Ir_4Si_{10}$ [2] suggests that the ordered phase is described by a low dimensional model. Such a small critical value β is considered as justification of the two dimensional behavior.

The key features of Peierls' model observed in the quasi 1D conductors include a Kohn anomaly in phonon spectra, a structural transition and a metal-insulator transition [9-15]. This model is characterized by a weak electron-phonon interaction. Contrary to the low dimensional charge density wave systems, the ordered state established in $Lu_5Ir_4Si_{10}$ has a three dimensional character. $Lu_5Ir_4Si_{10}$ crystallizes in the P4/mbm tetragonal space group and presents a complex three dimensional structure including one dimensional lutetium chains along the crystallographic c axis with a strong inter-chain coupling (Fig. 1) [8]. The CDW transition in $Lu_5Ir_4Si_{10}$ could be related to the existence of 1D Lu chains. Competition between CDW and superconductivity ordering occurs below 4 K. Transition metal dichalcogenides have been the center of CDW research but the results are still confusing [10-13]. McMillan [14] proposed a description beyond the weak coupling limit to explain the anomalies observed in 2H-$TaSe_2$. The question is why the T_S transition in $Lu_5Ir_4Si_{10}$ is attributed to a charge density wave transition.

The elastic constants are thermodynamic derivatives. They are important together with the specific heat and thermal expansion for the equation of state of a material [16, 17]. Following our survey of the thermodynamic properties of the charge density wave systems [18] we reexamine the Landau phenomenological approach for $Lu_5Ir_4Si_{10}$ [14].

Complete elastic tensor of $Lu_5Ir_4Si_{10}$ is given in [6]. This system having a tetragonal symmetry is characterized by six independent, longitudinal C_{11}, C_{33} and shear C_{44}, C_{66}, C_{12}, C_{23} elastic stiffness constants. In this paper measurements of the velocity and attenuation of the elastic modes C_{11}, C_{33}, C_{44} and C_{66} on a high quality single crystal are reported.

2. Experiment

A single $Lu_5Ir_4Si_{10}$ crystal was grown in a tri-arc furnace by a Czochralski technique (see [7] for more details). The sample is a small parallelepiped crystal with dimensions $2\times1.5\times1$ mm^3. The largest dimension is along the c axis the other dimensions are along the a and b axes. The crystallographic axes were identified by X-ray diffraction. Laue diffraction measurements were made using the back-scattering X-ray diffraction technique on a PAN analytical PW 3830 diffractometer. The quality of the sample used for this study was checked and the pattern illustrated by Fig. 2 insured that the crystal presents a single crystalline domain.

The sample was annealed at 900 °C for 7 days under ultrahigh vacuum to reduce internal stress.

The pulse echo technique [19] was used at frequencies 15 and 45 MHz with bonded $LiNbO_3$ transducers to measure the velocity and ultrasonic attenuation of the elastic modes. The relative sound velocity $\Delta V/V$ was measured by a phase coherent detection as a function of temperature.

Ultrasonic elastic modes were generated into the crystal, k and u represent the

ultrasound propagation direction and polarization. Pure longitudinal modes C_{11} (k//u//axis a) and C_{33} (k//u//axis c) were generated along the a and c axes respectively. Shear modes

C_{44} (k//c, u//a) and C_{66} (k//a, u//b) were generated along the c and a axes respectively. Each elastic constant C_{ii} is related to the corresponding longitudinal or shear velocity V_{ii} by $C_{ii} = \rho V_{ii}^2$, i=1,3,4,6, (tetragonal symmetry) where ρ is the mass density $\rho=9$ g cm^{-3}.

3. Results

The temperature dependences of the relative velocities [ΔV(T)-V(50K)]/V(50K) and attenuations of the longitudinal C_{11}, C_{33} and the shear C_{44}, C_{66} modes are shown in Fig. 3-6.

The measurements have been extended to 10 K for the longitudinal C_{11} mode.

Our results are in qualitative agreement with the previous analysis [6]. The anomaly observed for the C_{11} at T_C~80 K phase transition in Fig. 3(a) is comparable with the anomaly reported in [6]. A small thermal hysteresis of about 1 K found between heating and cooling (Fig. 5 and 6) is in agreement with that observed with the electrical resistivity measurements [7]. The phase transition occurs at T_C ~80 K on cooling and at T_H ~81 K on heating. A step like decrease $\Delta V/V$ ~0.005 of the velocity of the longitudinal C_{11} mode and a minimum $\Delta V/V$ ~0.003 of the velocity of the longitudinal C_{33} is observed at T_C (Fig. 3 (a)). Steplike increases of the velocities of the shear C_{44} and C_{66} modes are observed at T_C (or T_H) (Fig. 3(b)). Below T_C the deviations $\delta V/V$ defined by $\Delta V/V-\Delta V_0/V_0$ where $\Delta V_0/V_0$ is the extrapolated linear dependence of the background velocities (black dotted line in Fig. 3 (a)) is shown for the C_{11} mode in Fig. 5.

We evaluate the elastic constant decreases ΔC_{11} at T_C from the mean field specific increase ΔC_P^{MF} [5] using the Ehrenfest relation and the discontinuity in the thermal expansion coefficient $\Delta\alpha \sim 2\times10^{-6}$ K^{-1} measured in [3]. The Ehrenfest relation established for a second order phase transition is given by [17].

$$\Delta C_{11}/C_{11}^2 \sim -V_m T_{CDW} \Delta\alpha^2/\Delta C_P^{MF} \qquad (1)$$

eq.1 gives $\Delta C_{11} / C_{11} \sim 0.004$ close to the experimental value (Fig. 3 (a) and table 1)

with the longitudinal elastic constant C_{11} ~230 GPa [6]. The measured specific anomaly at the CDW phase transition was analyzed by Kuo et al [5] by a small mean field term

ΔC_P^{MF} = 6 J/molK and a large contribution due to fluctuations. The molar volume is

$V_m = 2x10^{-4}$ m^3/mol.

In conclusion the Ehrenfest mean field theory relationship (eq. 1) is satisfied at the T_C phase transition in $Lu_5Ir_4Si_{10}$. In the same manner, the Ehrenfest relationship is satisfied by several CDW compounds such as the quasi-one-dimensional conductor $K_{0.3}MoO_{0.3}$ [20], the transition metal dichalcogenide compound 2H-$NbSe_2$ and the rare earth tritellurides compounds $TbTe_3$, $ErTe_3$ and $HoTe_3$ [18].

4. Analysis

4.1 Landau theory of a second order phase transition

The interpretation of the elastic constants is based on an expansion of the free energy density in powers of the strain components e_i and the order parameter Q with the mean field approximation. In a second order transition, the Landau free interaction energy has the form [14, 21, 22]:

$$F(e_i,Q)= F_0 + a(T-T_0)Q^2/2 + cQ^4/4 + C_{11,0}e_1^2/2 + C_{33,0}e_3^2/2 + (g_1e_1+ g_3e_3)Q^2 + (h_1e_1^2+h_3e_3^2)Q^2 \quad (2)$$

where a is positive, $C_{11,0}e_1^2/2 + C_{33,0}e_3^2/2$ is the elastic background energy at Q=0, g_i and h_{ii} are the coupling constants. A model was proposed by McMillan for the charge density waves in transition metal dichalcogenides with charge density as an order parameter [14]. The transition from the normal to the incommensurate state is second order.

The order parameter that minimizes the free energy [21] at $T<T_C$ is $Q = (a/c)^{0.5} (T_C-T)^{0.5}$

At a CDW phase transition the longitudinal strain components couples with the square power of the order parameter Q.

The new elastic constants are given by [22]

$C_{ii} = C_{ii,0} - [d^2 F/ dQdei] \chi_Q$ (3)

where $\chi_Q = [d^2F/dQ^2]^{-1}$ denotes the order parameter susceptibility.

It results that a decrease of C_{11} and C_{33} (velocities) occurs at a second order phase transition [22]:

$C_{11} = C_{11,0} - 2g_1^2/c$ and $C_{33} = C_{33,0} - 2g_3^2$ (4)

4.2 *Landau theory of a first order phase transition*

A cubic term is included by McMillan to describe the first order incommensurate-commensurate phase transition [14]. The Landau free interaction energy has the form:

$$F(e,Q)=F_0 + a(T-T_0)Q^2/2 - bQ^3/3 + cQ^4/4 + C_{11,0}e_1^2/2 + C_{33,0}e_3^2/2 + (g_1e_1 + g_3e_3)Q^2 +$$

$$(h_1e_1^2 + h_2e_3^2)Q^2 \qquad (5)$$

Minimizing energy F with respect to Q one observes than three temperatures are defined [21]

1) T_0 is the transition equilibrium temperature.

2) Below $T_H \sim T_0+9b^2/4ac$ the state is metastable.

3) Below $T_C \sim T_0+2b^2/ac$ the order parameter Q increases discontinuously in the ordered phase.

4) Above T_H the order parameter is zero, Q=0.

The thermal hysteresis is given by T_H-T_C~ b^2/ac.

Below T_C the solution of dF/dQ=0 gives the order parameter

$$Q = b/c + (a/c)^{0.5} (T_C-T)^{0.5} \quad (6)$$

A small thermal hysteresis T_H-T_C induces that the cubic coefficient b is small compared to the coefficient of the quartic term c.

$Q(0)^2 \sim aT_C/c$ is deduced from eq. 6. It results that $(T_H-T_C)/T_C \sim b^2/ac$ taking Q(0)=1

A small parameter T_H-T_C of about 1 K with T_C ~80 K in the case of $Lu_5Ir_4Si_{10}$ yields a ratio

b/c ~ 0.1.

The decrease of the elastic stiffness around T_C is now given by

$$C_{11} \sim C_{11,0} - 2g_1^2/c - g_1^2 (b/c)(ac)^{-0.5} (T_C-T)^{-0.5} \quad \text{and}$$

$$C_{33} \sim C_{33,0} - 2g_3^2/c - g_3^2 (b/c)(ac)^{-0.5} (T_C-T)^{-0.5} \quad (7)$$

T_C is the limit of metastability of the high temperature phase. On the contrary T_H is the limit of metastability of the low temperature phase. Critical behaviors appear at T_C and T_H during cooling and heating respectively. The transition takes place at the spinodal points (T_C, T_H) where the nucleation barriers vanish [21].

Below T_C

In the ordered phase, the coupling terms $h_1 e_1^2 Q^2$ yields that the temperature dependence of

the velocity of the C_{11} mode follows the temperature dependence of the order parameter

$\Delta V/V \sim h_1 Q^2$ as explained in [22].

Below T_C in the ordered phase the velocity of C_{11} (Fig. 5) increases continuously with decreasing temperature as

$$\delta V/V = (\delta V/V)_0(1-T/T_C)^{2\beta} \quad (8)$$

with $2\beta \sim 0.5$. This value is larger than the value 0.3 deduced from the temperature dependence of the intensities of the satellite reflections [2]. The dashed black line represents the temperature dependence of the square of the BCS order parameter [23]. Discrepancies with the BCS behavior exist in the range $0.7<T/T_C<1$.

4.3 Relaxation mechanism

In the ordered phase, a relaxation mechanism takes place (Landau Khalatnikov) with a relaxation time τ_{LK}. The ultrasonic attenuation at a measuring frequency ω is given by [16]:

$$Att = 2\, Att_{max}\, \omega\tau_{LK} /\{ (1 + (\omega\tau_{LK})^2\} \quad (9)$$

where $Att_{max} \sim \Delta v\omega/V^2$ is the attenuation maximum obtained at a temperature T_M when $\omega\tau_{LK}=1$. $A_{tte,max}$ increases with frequency (15 - 47 MHz Fig. 5).

τ_{LK} follows the critical temperature dependence $\tau_{LK} = \tau_{LK}^0 (1- T/T_C)^{-1}$ during cooling and

$\tau_{LK} = \tau_{LK}^0 (1- T/T_H)^{-1}$ during heating. Notice that T_M decreases when ω increases. The sharp variation of the attenuation just below T_C (T_H) is well described by eq. 12 (Fig. 5). The temperature dependence of the velocity and attenuation depends on the temperature scanning rate R. For clarity all the measurements are not shown.

The values of τ_{LK}^0 obtained at different temperature scanning rates are shown in Fig. 7. It results that the parameter τ_{LK}^0 depends on the temperature scanning rate R (K/min). We verify the scalling law [24] :

$$\tau_{LK}^0 \sim \tau_{LK}^0(0) + AR^n \qquad (10)$$

where A is a constant coefficient. Taking n=1 a least square fit of the τ_{LK}^0 data gives the value $\tau_{LK}^0(0) = 3.1\times10^{-12}$ s (black dashed curve) Fig. 7.The experimental τ_{LK}^0 data can also be described with n approaching 2/3 the universal value of the theoretical models [24] and a least square fit gives $\tau_{LK}^0(0) = 3.5\times10^{-12}$ s (blue curve in Fig 7) . The experimental accuracy does not permit to conclude between the two values, 1 or 2/3, of the exponent n.

Hysteresis is related to nucleation lags in a first order phase transition and consequently hysteresis depends on the rate of the temperature sweep [24]. Such an effect explains that the apparent relaxation time τ_{LK}^0 involved in the ultrasonic attenuation is related to the temperature scanning rate R (eq. 10). The parameter $\tau_{LK}^0(0)$ defined at R ~ 0 is the intrinsic relaxation time of fluctuations at the transition.

4.4 Comparison with 1D and 2D CDW systems

We compare in Fig. 8 the decrease of the velocity of the longitudinal mode C_{11} of $Lu_5Ir_4Si_{10}$ at the structural phase transition T_S ~ 80 K with the decrease of the velocity of the longitudinal modes at the CDW or Spin Density Wave (SDW) phase transitions in several materials: the quasi one dimensional conductor $K_{0.3}MoO_3$ [23] and the 2D rare earth tritelluride compounds RTe_3 (R=Tb, Er and Ho) [18], metal transition dichacogenide compounds 2H-$NbSe_2$ [26] and $TiSe_2$ (characterized by a structural transition T_S=200 K) [27], (SDW materials) Spin Peierls compound $CuGeO_3$ [28] and Cr [29].

The decrease of the velocity of the longitudinal C_{11} mode at the CDW phase transition in $Lu_5Ir_4Si_{10}$ is very similar to the decrease of the velocity of the longitudinal C_{33} mode observed

with the 2D rare earth tritelluride compounds ($TbTe_3$, $ErTe_3$ and $HoTe_3$) and to the decrease of the Young modulus with the quasi-one-dimensional conductor $K_{0.3}MoO_3$ (Fig. 8 and Table 1).

The Landau coefficients a and c were calculated by Allender et al. [25] in one dimensional chain model using a weak coupling mean field description and they are found to be:

$$a = N(E_F)/T_{CDW} \text{ and } c= 0.1N(E_F)/k_B^2T_{CDW}^2 \qquad (11)$$

These values are nearly identical with the BCS case where $N(E_F)$ is the density of state per unit energy interval at the Fermi level. It is interesting to note that the Landau coefficients a and c depend on $T_{CDW:}$

$$a \sim 1/T_{CDW} \text{ and } c \sim 1/ T_{CDW}^2 \qquad (12)$$

It results that the decrease of the elastic constant ΔC_{11} at the transition increases as the square of the temperature T_{CDW} of the phase transition as

$$\Delta C_{11} \sim 2g_1^2/c \sim 2 g_1^2 k_B^2 T_{CDW}^2 / N(E_F) \qquad (13)$$

where g_1 is the coupling constant (eq.4).

A remarkable feature is that $\Delta V/V$ ($\Delta V/V= \Delta C_{11}/2C_{11}$) exhibit a T_{CDW}^2 dependence in the Landau approach.

The steplike decreases $\Delta V/V$ of the velocity of the longitudinal C_{11} or C_{33} mode measured at the CDW (SDW) phase transition show effectively a T_{CDW}^2 (red dotted line) observed for all the materials reported (Fig. 8) :

$$\Delta V/V= 6.2x10^{-7}T_{CDW}^2 \qquad (14)$$

The experimental decrease $\Delta V/V$ obtained with $Lu_5Ir_4Si_{10}$ is in agreement with eq. 14. This result yields that the longitudinal elastic anomaly observed at the structural phase transition in $Lu_5Ir_4Si_{10}$ is similar to that observed at the charge density wave transitions in 1D and 2D systems.

There are some discrepencies between the absolute measured values of the elastic longitudinal constants in RTe3 (~50 GPa), $K_{0.3}MoO_3$ (~250 GPa) and $Lu_5Ir_4Si_{10}$ (~230 Gpa) table 1 in consequence to reduce this effect we report the relative values of the velocity in Fig. 8.

4 **Conclusions**

From evaluating sound velocity and attenuation measurements we arrive at the following conclusions.

The structural phase transition T_S in $Lu_5Ir_4Si_{10}$ is weakly first order with a decrease of the longitudinal C_{11} and C_{33} elastic constants, showing an apparent second order behavior. The decrease of the longitudinal elastic constants C_{11} and C_{33}, discontinuity in the thermal expansion coefficient and mean field specific heat contribution are in agreement with the Ehrenfest mean field theory relationship. In contrast the C_{44} and C_{66} modes exhibit a step discontinuity upward on cooling which is a first order transition behavior.
The C_{11} and C_{66} modes are sensitive to changes in the a, b crystallographic plane. The longitudinal C_{11} and shear C_{66} modes having both the propagation and displacement in the a, b plane are strongly coupled to the ordering system. The microscopic model of the CDW phase transition $Lu_5Ir_4Si_{10}$ is not yet well known. Similarities are found between the longitudinal elastic anomalies at the structural phase transition T_S in $Lu_5Ir_4Si_{10}$ with the longitudinal elastic anomalies observed at the charge density wave transitions in the 2D rare earth tritelluride compounds $TbTe_3$, $ErTe_3$, $HoTe_3$, in the quasi one dimensional conductor $K_{0.3}MoO_3$ and in the 2D metal transition dichalcogenide 2H-$NbSe_2$. The microscopic model of the CDW phase transition in $Lu_5Ir_4Si_{10}$ is not yet well known. The present results suggest that

the nature of the structural phase transition T_S in $Lu_5Ir_4Si_{10}$ is associated to a classical Landau phase transition.

References

[1] B. Becker, N. G. Patil, S. Ramakrishnan, A. A. Menovsky, G. J. Nieuwenhuys, J.A. Mydosh,
Strongly coupled charge-density wave transition in single-crystal $Lu_5Ir_4Si_{10}$
Phys. Rev. B 59 (1999) 7266-7269. doi: 10.1103/PhysRevB.59.7266.

[2] S. Van Smaalen, M. Shaz, L. Palatinus, P. Daniels, F. Galli, G. J. Nieuwenhuys, J. A. Mydosh,
Multiple charge-density-waves in $R_5Ir_4Si_{10}$ (R=Ho, Er, Tm, and Lu)
Phys. Rev. B 69 (2004) 014103. doi: 10.1103/PhysRevB.69.014103.

[3] C. A. Swenson, R. N. Shelton, P. Klavins, H. D. Yang,
Thermal-expansion measurements for $Lu_5Ir_4Si_{10}$, $Lu_5Rh_4Si_{10}$, $Sc_5Ir_4Si_{10}$ and $Tm_5Ir_4Si_{10}$ charge- density-wave effects
Phys. Rev. B 43 (1991) 7668-7675. doi: 10.1103/PhysRevB.43.7668.

[4] R. N. Shelton, L. S. Hausermann-Berg, P. Klavins, H. D. Yuang, M. S. Anderson, C. A. Swenson,
Electronic phase transition and partially gapped Fermi surface in superconducting $Lu_5Ir_4Si_{10}$ Phys. Rev. B 34 (1986) 4590-4594. doi: 10.1103/PhysRevB.34.4590.

[5] Y.-K. Kuo, C. S. Lue, F. H. Hsu, H. H. Li, H. D. Yang
Thermal properties near the charge-density-wave transition
Phys. Rev. B 64 (2001) 125124. doi: 10.1103/PhysRevB.64.125124.

[6] J. B. Betts, A. Migliori, G. S. Boebinger, H. Ledbetter, F. Galli, J. A. Mydosh,
Complete elastic tensor across the charge density wave transition in monocrytal $Lu_5Ir_4Si_{10}$
Phys. Rev. B 66 (2002) 060106 (R). doi: 10.1103/PhysRevB.66.060106.

[7] M. Leroux, P. Rodiere, C. Opagiste,
Charge-density-wave properties in single crystal of $Lu_5Ir_4Si_{10}$
J. Superconductivity and Novel Magnetism 26 (2012) 1669. doi: 10.1007/s10948-12-1860-2.

[8] B. Mansart, M. J. G. Cottet, T. J. Penfold, S. B. Dugdale, R. Tediosi, M. Chergui, F. Carbone.
Evidence for a Peierls phase transition in a three-dimensional multiple charge-density waves in solid.
Proc. Natl. Acad. Sci. (2011) doi : 10.1073/pnas.1117028109.

[9] M. D. Johannes, I. Mazin,
Fermi Surface nesting and the origin of charge density waves in metals
Phys. Rev B 77 (2008) 165135; doi.org/10.1103/PhysRevB77.165135.

[10] X. Zhu, J. Guo, J. Zhang, E. W. Plummer, J. D. Guo
Classification of charge density waves based on their nature
Proc. Natl. Acad. Sci. 112 (2015) 2367-2371; doi:101073/pnas-1424791112.

[11] X. Zhu, J. Guo, J. Zhang, E. W. Plummer,
Misconception associated with the origin of charge density waves
Adv. Phys. 2 (2017) 622-640. doi.org /10.1080/23746149.2017.1343098

[12] S. Manzeli, D.Ovchinnikov, D. Pasquier, O. V. Yazyev, A. Kis
2D transition metal dichacogenides
Nature Reviews/Materials 2 (2017) 17033; doi 10.1038/natrevmats.2017.33.

[13] J. A. Wilson, F. Di Salvo, S. Mahajan
Charge density waves and superlattices in the metallic layered transition metal
Advances in Physics 24 (1975) 117. doi: 10.1088/0031-8949/91/5/053009.

[14] W. L. McMillan
Landau theory of charge density waves in transition-metal dichalcogenides
Phys. Rev. B 12 (1975) 1187-1196. Doi: 10.1103/PhysRevB.12.1187.

[15] S.B. Dugdale
Life on the edge: a buginner's guide to the Fermi Surface.
Phys. Scr. 91, 063009 (2016). doi: 10.1088/0031-8949/91/5/053009.

[16] B. Lüthi in **Physical Acoustics in the solid state** Solid State Sciences

ed. M. Cardona et al. Springer-Verlag (2005)

[17] L. R. Testardi,
Elastic modulus, thermal expansion, and specific heat at a phase transition
Phys. Rev. B 12 (1975) 3849-3853. doi: 10.1103/PhysRevB.12.3849.

[18] M. Saint-Paul and P. Monceau,
Survey of the thermodynamic properties of the charge density wave systems
Advances in condensed matter (Hindawi) (2019) 2138264; doi /10.1155/2019/2138264

[19] M. Saint-Paul, C. Guttin, P. Lejay, G. Remenyi, O. Leynaud, P. Monceau
Elastic anomalies at the charge density wave transition in $TbTe_3$.
Solid State Commun.233 (2016) 24-29.doi: 10.1016/j.ssc.2016.02.008.
and
Elastic anomalies at the charge density wave transition in $HoTe_3$.
International Journal of Modern Physics B 32 52018) 1850249
doi:10.1142/S0217979218502491.
and
Elastic anomalies at the charge density wave transition in $HoTe_3$.
International Journal of Modern Physics B 32, 1850249 (2018).
doi:10.1142/S0217979218502491.

[20] J. W. Brill, M. Chung, Y.-K. Kuo, E. Figueroa, G. Mozurkewich
Thermodynamics of the Charge-Density-Wave Transition in Blue Bronze,
Phys. Rev. Lett. 74 (1995) 1182. doi:10.1103/PhysRevLett.74.1182.

[21] L. Landau and E. Lifshitz, Statistical Physics, Pergamon Press, 1968
and K. Binder,
Theory of first order phase transitions
Rep. Prog. Phys. 50 (1987) 783859. doi.org/10.1088/0034-4885/50/7/001

[22] W. Rehwald ,
The study of structural phase transitions by means of ultrasonic experiments
Adv. Phys. 22 (1973) 721-755. doi/10.1080/00018737300101379.

[23] G. Gruner,
Density Waves in Solids

ed. D. Pines (Addison-Wesley) 1994.

[24] F. Zhong, J. Zhang,
Scaling of hysteresis with temperature scanning rate
Phys.Rev. E 51 (1995) 2898-2901. doi: 10.1103/PhysRevE.51.2898.

[25] D. Allender, J. W. Bray, J. Bardeen,
Theory of fluctuation superconductivity from electron phonon interactions in pseudo-one-dimensional systems.
Phys. Rev. B 9, 119(1974).

[26] M. H. Jericho, A. M. Simpson, R. F. Frindt**,**
Velocity of ultrasonic waves in 2H-$NbSe_2$, 2H-TaS_2 and 1T-TaS_2
Phys. Rev B 22, 4907-4914 (1980).

[27] A. Caillé, Y. Lepine, M. H. Jericho, A. M. Simpson**,**
Thermal expansion, ultrasonic velocity and attenuation measurements in TiS_2,$TiSe_2$ and $TiS_{0.5}Se_{1.5}$
Phys. Rev. B 28, 5454 (1983).

[28] M. Saint-Paul, G. Reményi, N. Hegmann, P. Monceau, G.Dhalenne, A. Revcolevschi**,**
Ultrasonic Study o magnetoelastic effects in the spin -Peierls state of CuGeO3
Phys. Rev. B 52, 15298 (1995).

[29] D. I. Bolef, J. De Klerk**,**
Anomalies in the elastic constants and thermal expansion of chromium single crystals
Phys. Rev B 129, 1063-1067 (1963).

Table 1 Anomalies of Specific heat, thermal expansion and elastic constants at the T_S phase transition in $Lu_5Ir_4Si_{10}$ and at T_{CDW} in $TbTe_3$, $ErTe_3$ and $HoTe_3$. Molar volume V_m.

$Lu_5Ir_4Si_{10}$ **$V_m=2\times10^{-4}$ m^3**	**T_{CDW}~80 K** **Thermal expansion coefficient** **$\Delta\alpha=-2\times10^{-6}$ K^{-1} [3]**	**Specific heat jump** **ΔC_p=160J/molK [1]** mean fieldcontribution ΔC_P^{MF}=6J/molK [5] $\frac{\Delta C_P^{MF}}{T_{CDW}V_m} = a^2\frac{\Delta C_{11}}{2g_1^2}$	**Elastic constant decreases** **$\Delta C_{11}/C_{11}$=0.01** **$\Delta C_{33}/C_{33}$=0.006** **C_{11}~C_{33} ~230GPa[6]**
$TbTe_3$ **$V_m=7\times10^{-5}$ m^3** **$ErTe_3$** **$HoTe_3$**	**T_{CDW}=330 K** **$T_{CDW=}$260 K** **T_{CDW}=280 K**	**Specific heat jump** **ΔC_P=3 J/molK [19]**	**Elastic constant decrease** **$\Delta C_{33}/C_{33}$=0.02[19]** **$\Delta C_{33}/C_{33}$=0.03** **$\Delta C_{33}/C_{33}$=0.05** **C_{33}~50 GPa**
$K_{0.3}MoO_3$ **$V_m=3.6\times10^{-5}$ m^3**	**T_{CDW}=180 K**	**Specific heat jump** **ΔC_P=3 J/molK [20]**	**Young modulus[20]** **$\Delta Y/Y$=0.02** **Y~250 GPa**

Figure captions

Fig.1 color on line

Lu5Ir4Si10 (P4/mbm tetragonal space group) is constituted of 1D chains of first neighbour lutetium atoms along the $\vec{c}$ axis with a strong inter-chain coupling.

Fig. 2 color on line

Laue diffraction pattern of Lu5Ir4Si10 single crystal obtained with the incident X-ray beam aligned along the $\vec{c}$ axis. Inset the single crystal cut along the crystallographic axes.

Fig. 3 color on line

(a) Temperature dependence of the relative velocity of the longitudinal C_{11} (blue symbols) and C_{33} (black symbols) modes. Extrapolations $\Delta V_{back}/V_{back}$ of the linear temperature dependence of the background velocity above T_C and shifted to the minimum value at T_C (dashed black line), cooling measurements.

(b) Temperature dependence of the relative velocity of the shear C_{44} (black symbols) and C_{66} (blue symbols) modes, cooling measurements.

Fig 4 color on line

Temperature dependence $\delta V/V=\Delta V/V-\Delta V_{back}/V_{back}$ of the longitudinal C_{11} mode, where $\Delta V_{back}/V_{back}$ is the extrapolated high temperature background velocity shifted to the minimum value at T_C (dashed black line in Fig. 3a).

Red dashed curve is calculated with $\frac{\partial V}{V} = 0.01\left\{\left[1-\frac{T}{80}\right]^{0.5}\right\}$. Black dashed curve is calculated with $\frac{\partial V}{V} = 0.0065\left\{\left[\frac{Q(T)}{Q(0)}\right]^{2}_{BCS}\right\}$, temperature dependence of the square of the BCS order parameter $Q(T)/Q(0)_{BCS}^2$.

Fig. 5 color on line

(a) Temperature dependence of the relative velocity and attenuation of the longitudinal mode C_{33} measured at 15 MHz, heating at rate 0.15 K/min, cooling at rate 0.25K/min, attenuation (red curves fit) calculated using eq. 12 with $\tau_{LK}^{0}=1.3\times10^{-11}$ s (heating) and $\tau_{LK}^{0}=2.6\times10^{-11}$ s (cooling).

(b) Temperature dependence of the relative velocity and attenuation of the longitudinal mode C_{33} measured at 45 MHz, heating at rate 0.25 K/min, cooling at rate 0.3K/min, attenuation calculated (red curves fit) using eq. 12 with $\tau_{LK}^{0}=2\times10^{-11}$ s (heating) and $\tau_{LK}^{0}=2\times10^{-11}$ s (cooling).

Fig 6 color on line

(a) Temperature dependence of the relative velocity and attenuation of the shear C_{66} mode.

(b) Temperature dependence of the relative velocity and attenuation of the shear C_{44} mode.

Fig.7 color on line

Relaxation time τ_{LK}^{0} estimated at different heating and cooling rate R (K/min). The black and blue dashed lines are calculated with eq. 12 using n=1and n=2/3 respectively.

Fig.8 color on line

Relative velocity decrease of the velocity ($\Delta V/V$) the longitudinal C_{11} and C_{33} modes at the CDW phase transition as a function of the temperature of the phase transition T_{CDW}.

Quasi-one conductor $KoMoO_3$ (green circle) T_{CDW}=180 K [20]; Transition metal dichalcogenides 2H-$NbSe_2$ (blue square) T_{CDW}=30 K [26] and $TiSe_2$ (blue up triangle) Ts =200 K [27]; Rare earth tritellurides $ErTe_3$ (black down triangle) T_{CDW}=260 K [19], $TbTe_3$ (pink down triangle) T_{CDW}=330 K [19], $HoTe_3$ (blue down triangle) [19]. Intermetallic compounds $Lu_5Ir_4Si_{10}$ (red square) T_S=80 K; Spin Peierls systems $CuGeO_3$ (blue diamond) T_{SDW}=14 K [28]; chromium Cr (light blue diamond) T_{SDW}=310 K [29]. The calculated red dashed line $6.2x10^{-7}\ T_{CDW}^{2}$.

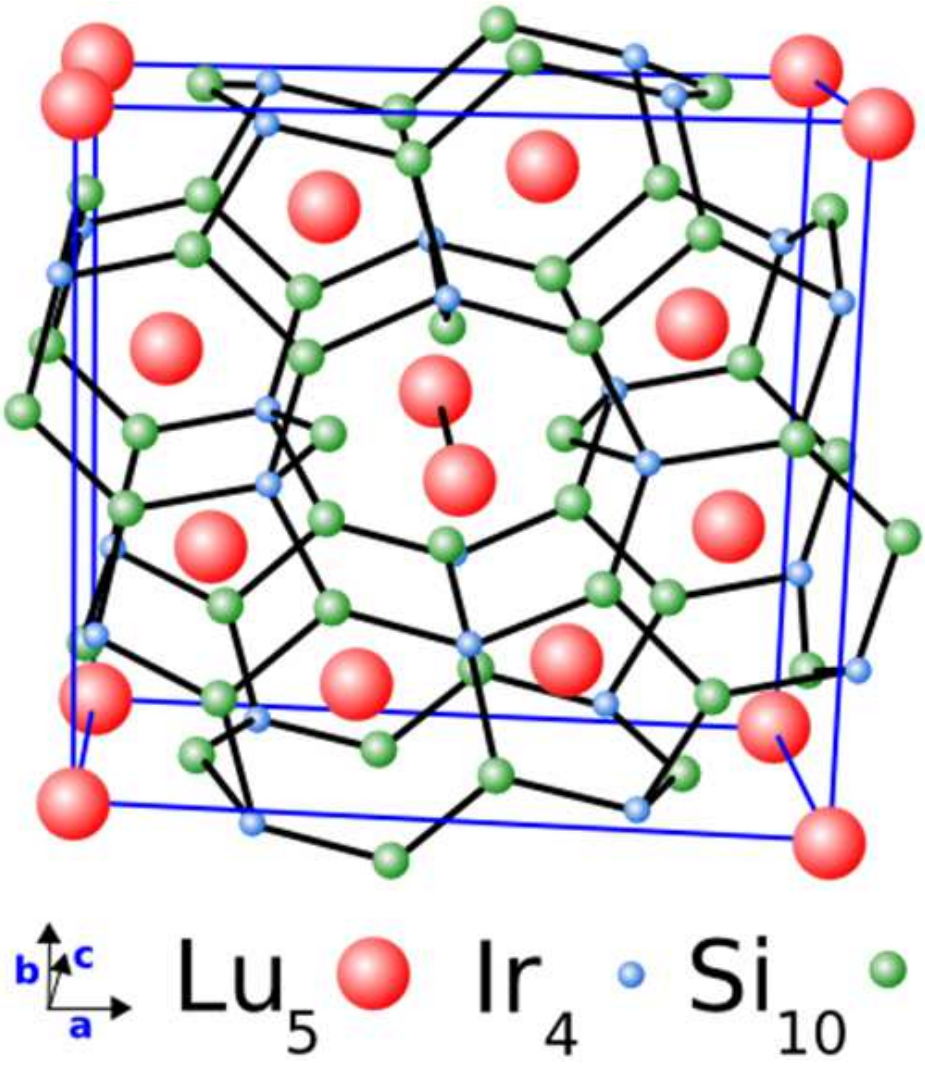

Fig1

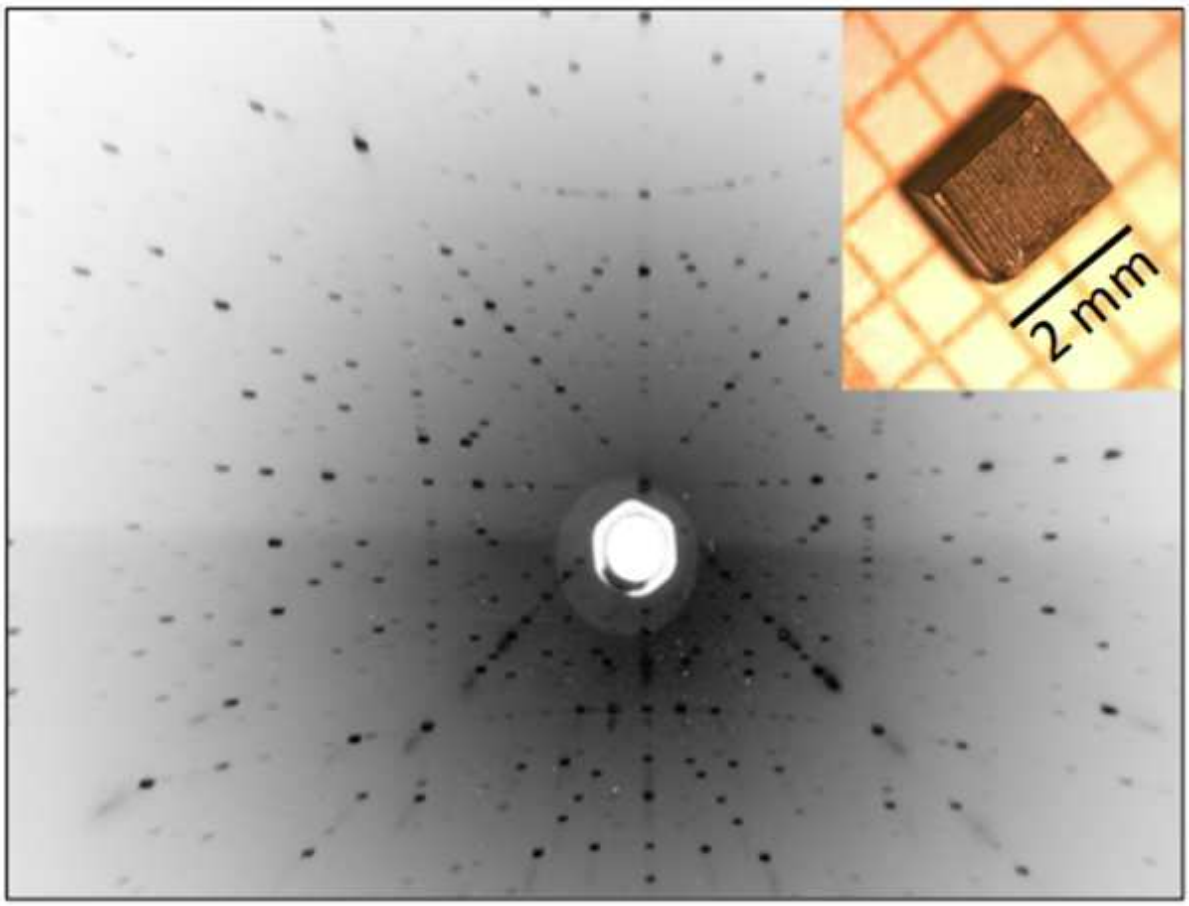

Fig2

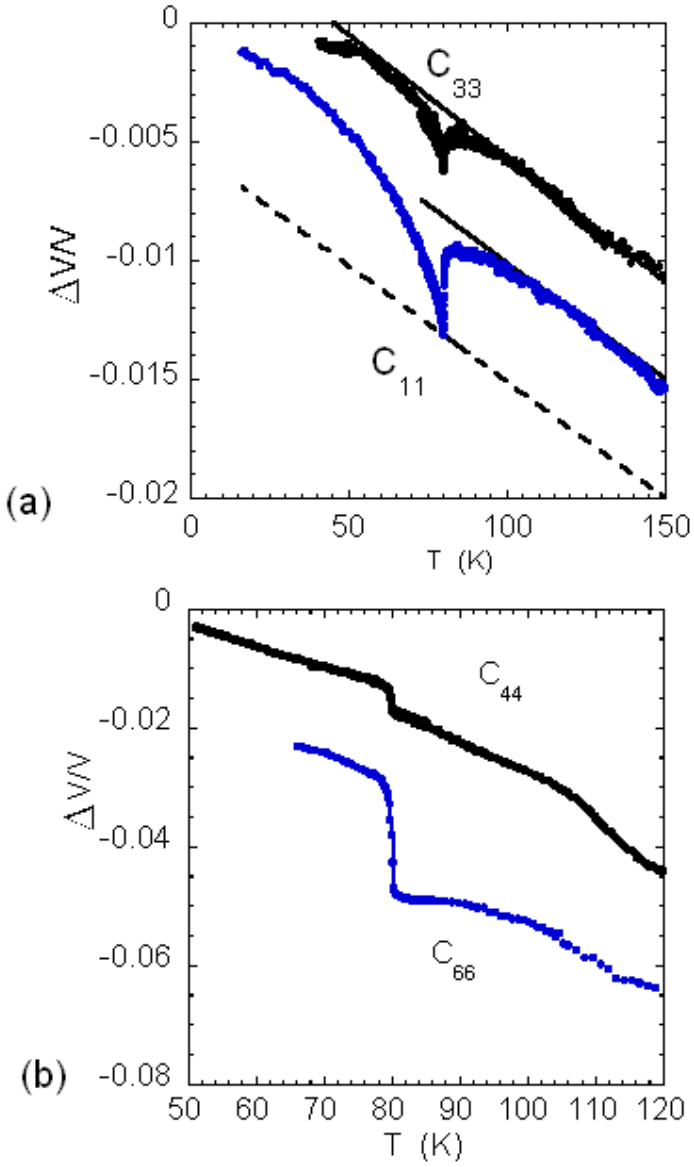
0
-0.005
-0.01
-0.015
-0.02
ΔV/V
C33
C11
(a)
0
50
100
150
T (K)
0
-0.02
-0.04
-0.06
-0.08
ΔV/V
C44
C66
(b)
50
60
70
80
90
100
110
120
T (K)

Fig3

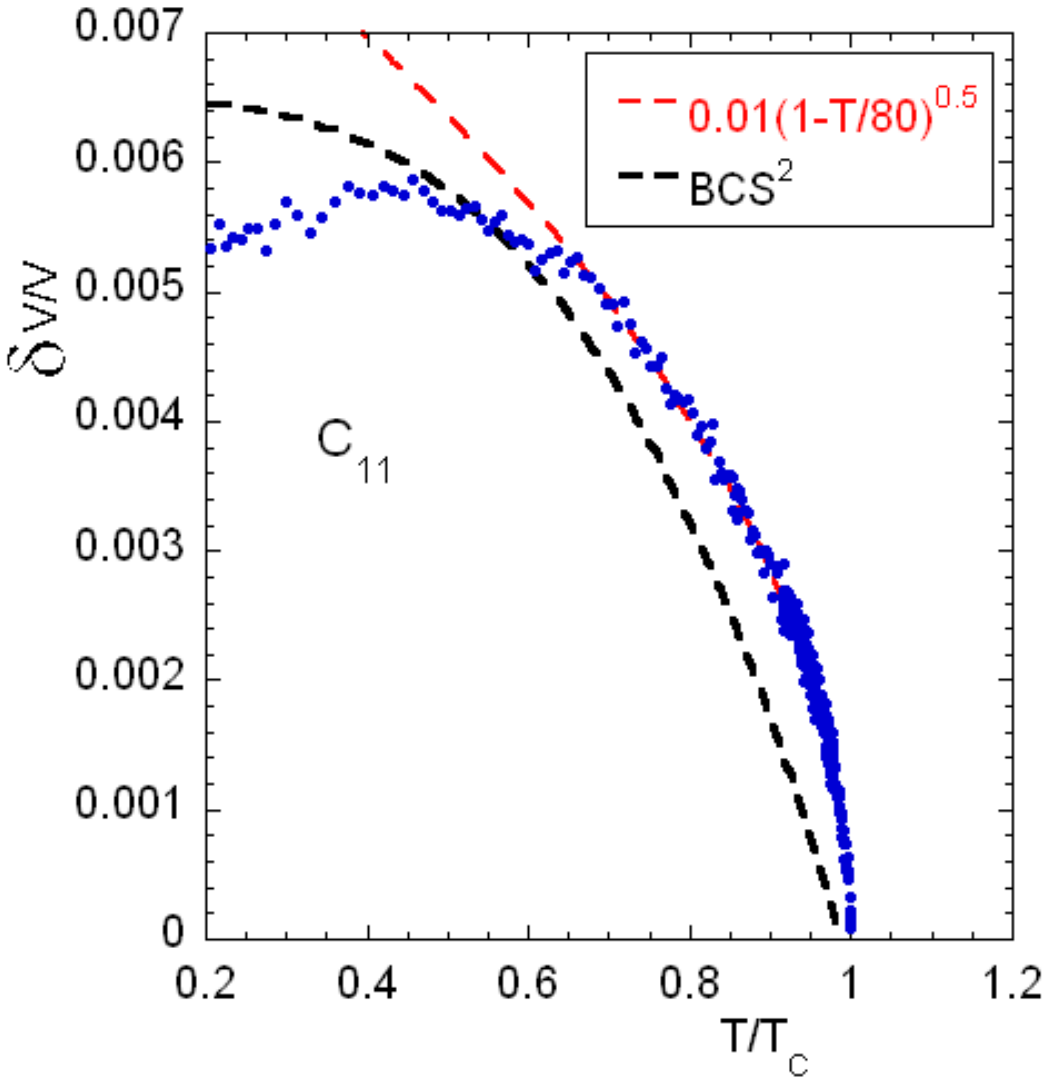
0.007
0.006
0.005
0.004
0.003
0.002
0.001
0
δV/V
0.2
0.4
0.6
0.8
1
1.2
T/T_C
0.01(1-T/80)^0.5
BCS^2
C11

Fig. 4

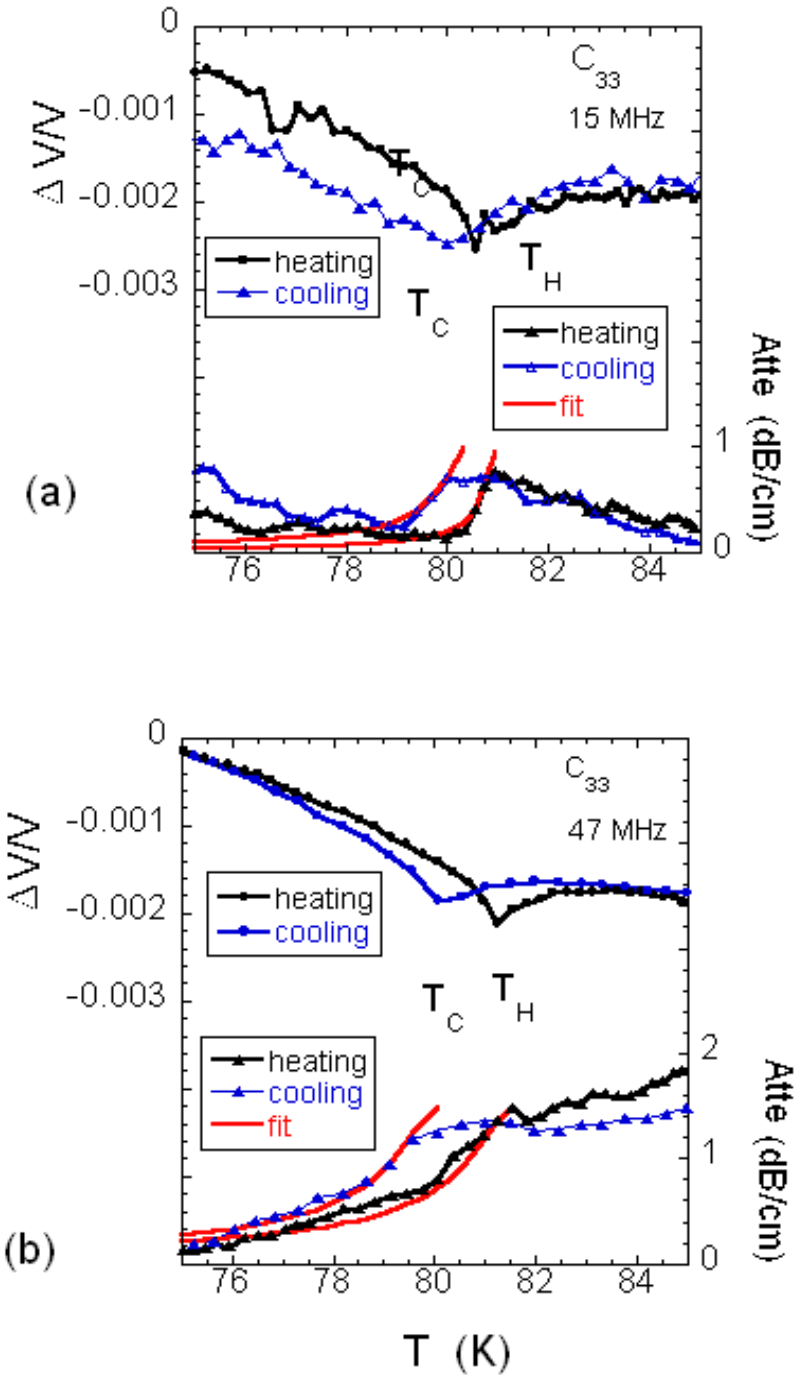
0
-0.001
-0.002
-0.003
ΔV/V
C33
15 MHz
heating
cooling
T_C
T_H
heating
cooling
fit
Atte (dB/cm)
1
0
(a)
76
78
80
82
84
0
-0.001
-0.002
-0.003
ΔV/V
C33
47 MHz
heating
cooling
T_C
T_H
heating
cooling
fit
2
1
0
Atte (dB/cm)
(b)
76
78
80
82
84
T (K)

Fig5

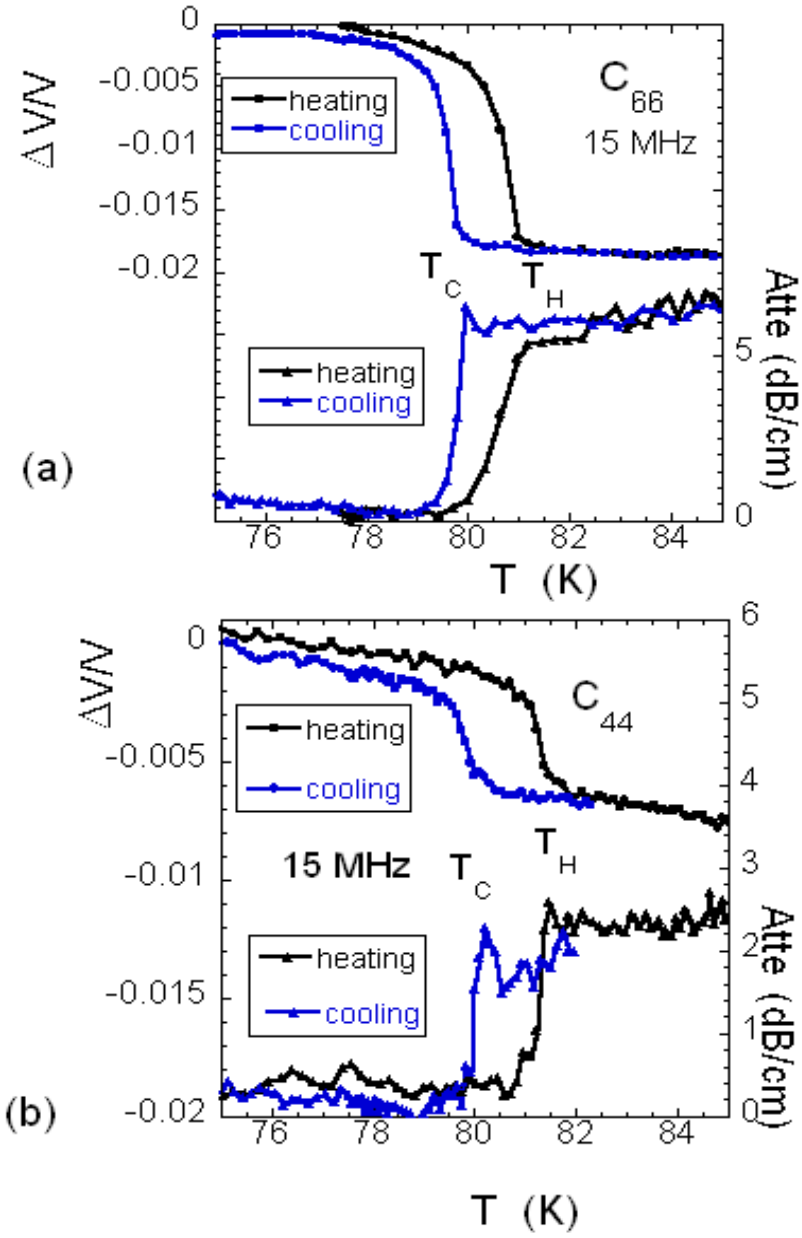
(a)
ΔV/V
0
-0.005
-0.01
-0.015
-0.02
heating
cooling
C66
15 MHz
T_C
T_H
heating
cooling
Atte (dB/cm)
5
0
76
78
80
82
84
T (K)
(b)
ΔV/V
0
-0.005
-0.01
-0.015
-0.02
heating
cooling
C44
T_H
15 MHz
T_C
heating
cooling
6
5
4
3
2
1
0
Atte (dB/cm)
76
78
80
82
84
T (K)

Fig6

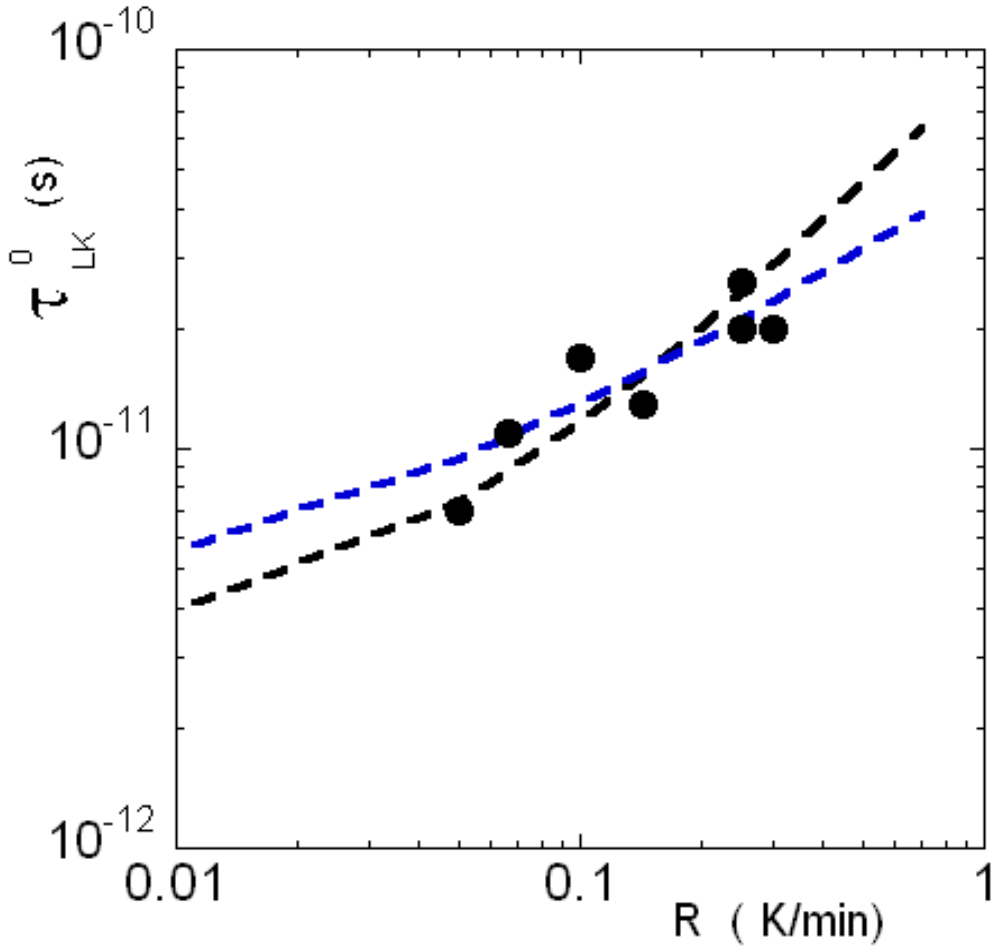

Fig 7

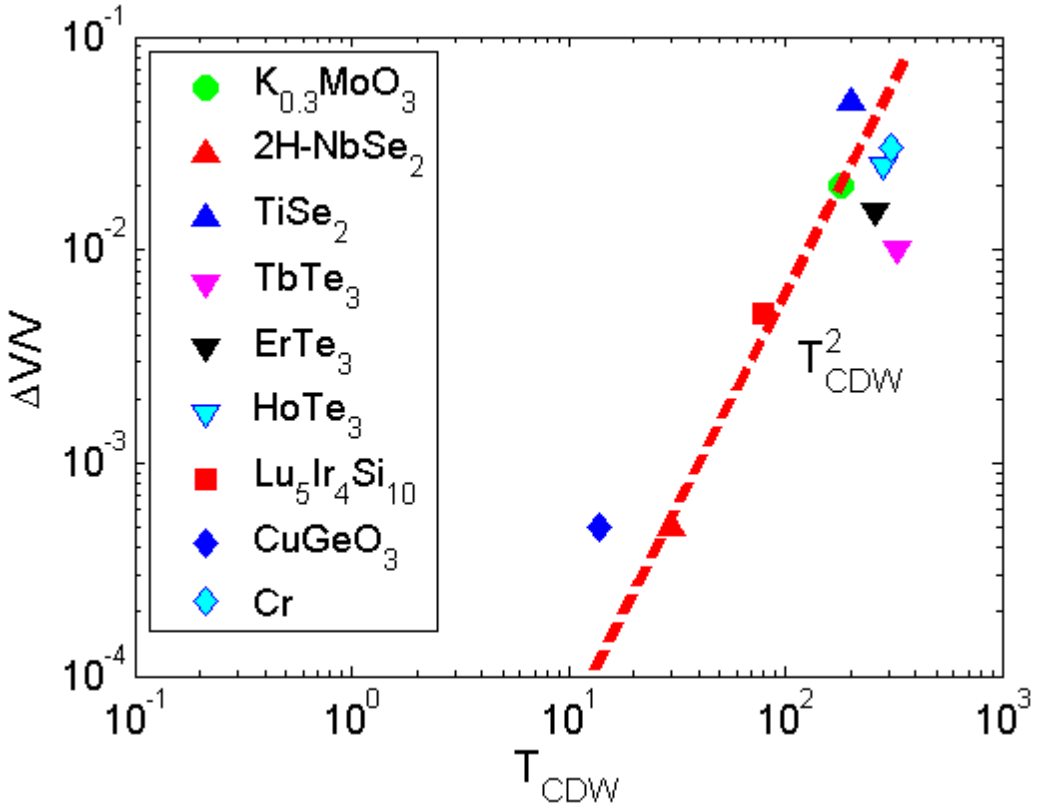
10^{-1}
10^{-2}
10^{-3}
10^{-4}
ΔV/V
10^{-1}
10^{0}
10^{1}
10^{2}
10^{3}
T_{CDW}
T^2_{CDW}
$K_{0.3}MoO_3$
2H-$NbSe_2$
$TiSe_2$
$TbTe_3$
$ErTe_3$
$HoTe_3$
$Lu_5Ir_4Si_{10}$
$CuGeO_3$
Cr

Fig. 8